Investigation Into the Integration of a Resonant Tunnelling Diode and an Optical Communications Laser: Model and Experiment

Thomas J. Slight and Charles N. Ironside

***Abstract*—A resonant tunnelling diode has been monolithically integrated with an optical communications laser [the resonant tunnelling diode (RTD-LD)] to form a simple optoelectronic integrated circuit (OEIC) that is a novel bistable device suitable for an optical communications system. The RTD-LD was based on a ridge-waveguide laser structure and was fabricated from an InAlGaAs–InP epi-wafer grown by molecular beam epitaxy; it emitted at around 1500 nm. Voltage controlled optical–electrical switching and bistability were observed during the characterisation of the RTD-LD – useful features for a fibre-optic communications laser.**

Optical and electrical simulations of the RTD-LD were carried out using the circuit simulation tool PSPICE. In addition, a discrete component version of the RTD-LD was constructed which exhibited optical power oscillations, and along with the results of the simulations, gave insight into the operating principles of the monolithically integrated RTD-LD.

***Index Terms*—Driver circuits, integrated optoelectronics, optical bistability, optical fiber communication, resonant tunneling diodes (RTDs), semiconductor lasers.**

I. Introduction

IN THIS PAPER, we report the use of a resonant tunnelling diode (RTD) [1] as a driver for a semiconductor laser to form a simple optoelectronic integrated circuit (OEIC) that is a novel alternative to traditional transistor based driver circuits [2]. The RTD acts as a voltage controlled switch for the laser, and causes the device (the RTD-LD) to become electrically/optically bistable, making it particularly convenient for nonreturn to zero (NRZ) digital modulation. Low voltage digital signals can be employed to switch the device between *on* and *off* states. Furthermore, the RTD and semiconductor laser are vertically integrated [3] and so only one epitaxial growth stage is required.

Previous work on the integration of tunnelling diodes and bipolar devices include the vertical integration of a Si–SiGe heterojunction bipolar transistor (HBT) and resonant interband tunnel diode (RITD) reported in [4], and the integration of a field effect transistor (FET) and RTD presented in [5]. Optoelectronic devices utilising the resonant tunnelling diode/effect include the resonant tunnelling light-emitting diode (RTLED) [6], the RTD electroabsorption modulator [7], the resonant tunnelling effect quantum-well laser [8] and the resonant tunnelling injection laser [9]. Grave *et al.* [10] have demonstrated an integrated RTD/laser in the GaAs–AlGaAs material system, and have demonstrated its application as an optical two state memory, but in this work we are targeting optical communications applications with the emphasis on increased functionality and an emission wavelength of around 1.55 μm. We have characterised the low frequency operation of the RTD-LD, demonstrated optical/electrical bistability, and modelled its electrical characteristics using PSPICE [11].

We previously reported some aspects of the operation of the integrated RTD-LD [12], here we give a more detailed account of the development of the device. This paper proceeds as follows; first we present work on a RTD-LD hybrid module where we separately characterise the RTD and laser diode. We connect these in series to form a hybrid integrated circuit (HIC) and then characterise the HIC. This approach allows us to build up, in a step by step fashion a model of the RTD-LD HIC. This model is verified by fitting the overall behavior of the RTD-LD HIC. We can then use the model to gain considerable insight into the operation of the monolithically integrated RTD-LD. We then discuss the wafer design, growth and fabrication of the integrated RTD-LD and use the model developed from the HIC work to model the results obtained from the the integrated RTD-LD. Finally, the conclusion includes a discussion of the implications of this work for OEIC development and further work required before this device can be implemented in an optical communications system.

II. RTD-LD Module

The RTD-LD module is an RTD/laser diode HIC with separate RTD and Laser components connected by a short bond wire. Generally, HICs are commonly used in optoelectronic transmitter modules and comprise of optoelectronic/electronic devices such as laser diodes and driver integrated circuits mounted in close proximity and connected via bond wires [13]–[15]. To the authors knowledge the RTD-LD module is the first HIC to combine a laser diode and an RTD.

The RTD component of the RTD-LD module was fabricated from preexisting RTD epimaterial that was originally used in the work described in [7]. The RTD devices were circular mesas of area 2000 μm^2 formed by wet etching using a metal mask which also served as the electrical contacts. The laser diode was a commercial prototype device[1] of the ridge waveguide design with a 5-μm ridge width. The laser was designed for continuous-wave (CW) room-temperature operation with emission at

Manuscript received November 16, 2006; revised February 19, 2007. The work of T. J. Slight was supported in part by the Engineering and Physical Sciences Research Council (EPSRC) in the form of a studentship.

The authors are with the Department of Electronics and Electrical Engineering, University of Glasgow, Glasgow G12 8LT, U.K. (e-mail: tslight@elec.gla.ac.uk; ironside@elec.gla.ac.uk).

Digital Object Identifier 10.1109/JQE.2007.898847

[1]Fabricated by Intense, a U.K. based manufacturer of laser array modules.

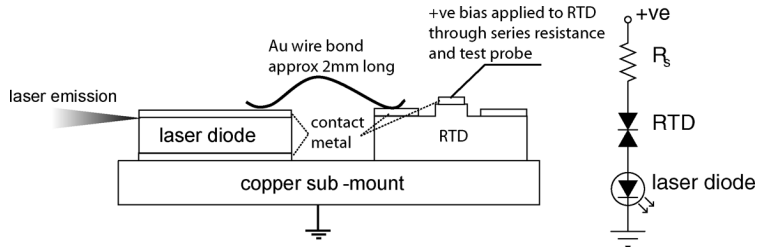

Fig. 1. Illustration of the RTD-LD module. The RTD and Laser dies are attached to the copper sub mount with silver epoxy, a wire bond is made between them using a wedge bonder. Alongside is shown the electrical schematic diagram of the resistance, RTD, and laser diode connected in series.

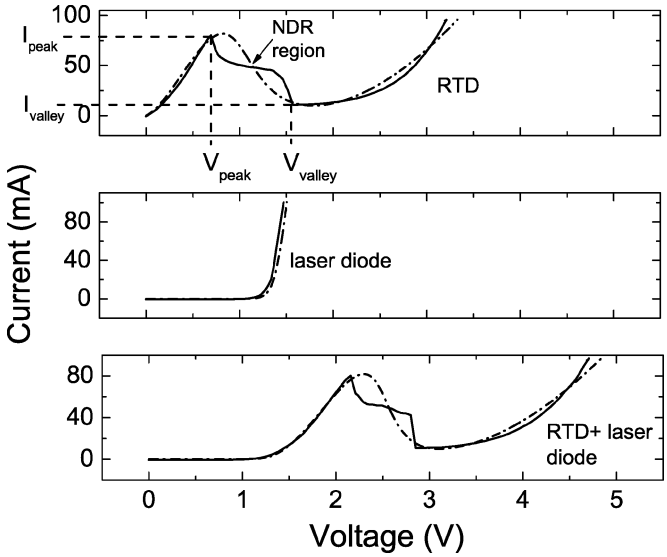

Fig. 2. Solid lines show the I–V characteristics for the RTD-LD module. Shown from top to bottom are the I–V characteristics for the RTD, the laser diode, and the RTD and laser diode connected in series. Dashed lines show the PSPICE model characteristics.

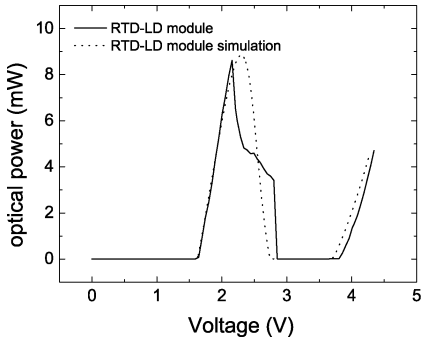

Fig. 3. $P_{\rm opt}$-V characteristic for the RTD-LD module. The optical power is oscillating over the range 2.2–2.8 V. The dotted line gives the result of the PSPICE simulation.

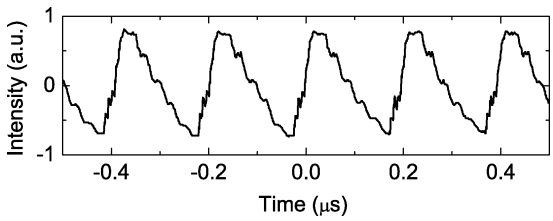

Fig. 4. Oscillations in the optical power from the hybrid device laser diode at a drive voltage of 2.54 V. The plot shows the positive and negative deviations from the average optical power. The repetition rate is 5 MHz.

a wavelength of 980 nm. The RTD and LD were attached to a small copper block using electrically conductive silver epoxy resin. A wire bond was then made between the LD and RTD, connecting the two electrically in series. The bond wire itself was gold and had a diameter of 25 μm. The device is illustrated in Fig. 1.

Fig. 2 shows the current versus voltage (I–V) characteristics of the discrete devices utilised in the RTD-LD module tested separately and together. Shown are the I–V characteristics (from top) for the RTD, the laser diode, and the RTD and laser diode connected in series. The effect of adding the laser diode in series with the RTD is to introduce an additional 1.3 V voltage drop to the individual RTD characteristic. Also shown in Fig. 2 are some important parameters for the RTD I–V characteristic. Rising from zero bias, the RTD current peaks at $I_{\rm peak}$ (= 80 mA), $V_{\rm peak}$ (= 0.69 V), before falling throughout the negative differential resistance (NDR) region to a valley at $I_{\rm valley}$ (= 11 mA), $V_{\rm valley}$ (= 1.57 V). The current increases again after the valley region. Fig. 3 shows the optical power vs voltage ($P_{\rm opt}$-V) for the RTD-LD module.

In the RTD negative differential resistance region there is a clear current/optical power "shoulder" at around 2.5 V (the current does not reduce suddenly but reaches a plateau before dropping steeply again). This is not in fact an intrinsic characteristic of RTDs, but arises as a result of oscillations caused by the interaction of drive circuit impedance and negative differential resistance [16], [17]. The current "shoulder" results from the Agilent source voltage meter averaging the oscillating signal from the RTD-LD module. These oscillations were observed (Fig. 4) in the optical output of the laser diode using a 100-MHz bandwidth Ge p-i-n detector in conjunction with a 37 dB amplifier and a Hewlett Packard 500-MHz bandwidth oscilloscope. The bandwidth of the measurement system was limited by the 100-MHz bandwidth of the amplifier.

The addition of 15 Ω series resistance causes the RTD-LD module current (Fig. 5) and optical power (Fig. 6) to become bistable at voltages between the valley voltage of 3.03 V and the peak voltage of 3.39 V, with a hysteresis loop 360 mV wide. The current and optical power switch abruptly from "on" to "off" states and "off" to "on" states at $V'_{\rm peak}$ and $V'_{\rm valley}$ respectively. The optical power on/off ratio or extinction ratio was 31 dB at a bias of 3.24 V.

To visualise why the RTD-LD module exhibits electrical and optical bistability with the presence of series resistance it is worth while considering the graphical technique of load line

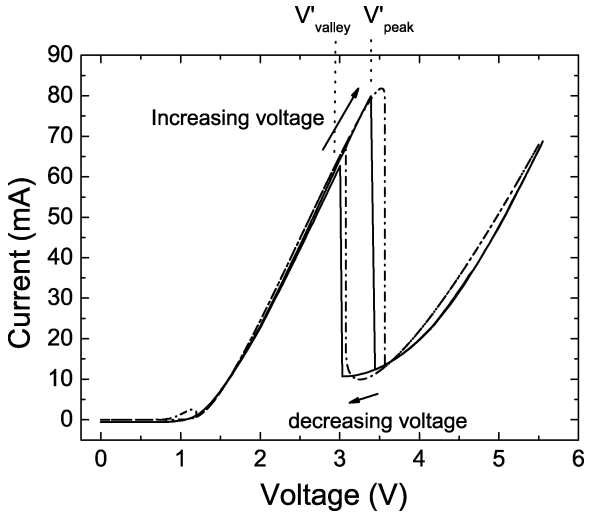

Fig. 5. Solid lines show the I–V characteristic for the RTD-LD module with the presence of a 15-Ω external series resistance. Switching points are labelled at $V'_{\rm peak}$ and $V'_{\rm valley}$. Dashed lines show the PSPICE model characteristics.

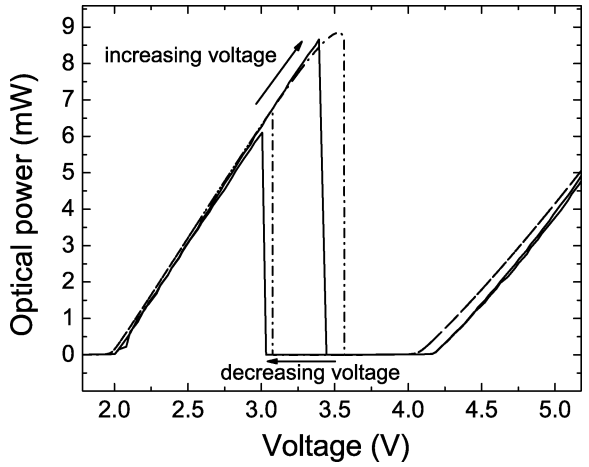

Fig. 6. Solid lines show the optical power versus voltage ($P_{\rm opt}$-V) characteristic for the RTD-LD module with 15-Ω external series resistance. The series resistance has caused the optical power to become bistable at voltages around 3.3 V, the hysteresis loop is 410 mV wide. Dashed lines show the PSPICE model characteristics.

analysis described in detail in [10]. The reason for the high extinction ratio observed is due to fact that the threshold current of the laser diode of 24 mA lies between the peak and valley currents of the laser ($I_{\rm peak} > I_{\rm th} > I_{\rm valley}$) such that the laser switches fully "on" or "off" at the $V'_{\rm peak}$ and $V'_{\rm valley}$ switching points.

PSPICE [11]—the general purpose analog circuit simulator—was used to model the dc characteristics of the RTD-LD module both with and without series resistance. The RTD-LD module is modelled by a series combination of resonant tunnelling diode, laser diode and resistance (shown schematically in Fig. 1). The RTD model was the one presented by Brown *et al.* [18], and was based upon the following equation representing the dc RTD I–V characteristic:

$$I = M \cdot (C_1 V^i \left\{\tan^{-1}\left[C_2\left(V - V_T\right)\right]\right\} - \left\{\tan^{-1}\left[C_2\left(V - V_N\right)\right]\right\} + C_3 V^j + C_4 V^k. \quad (1)$$

TABLE I
RTD MODEL PARAMETERS USED IN (1) FOR THE RTD-LD MODULE PSPICE MODEL

RTD model parameter	Value
i	1
j	2
k	1
C1	0.075
C2	3.215
C3	0.023
C4	-0.051
V_T	0V
V_N	1.01V
Scale	1

TABLE II
LD MODEL PARAMETERS USED FOR THE RTD-LD MODULE PSPICE MODEL

LD model parameter	Value
RP	0.362
$C_{P_{opt}}$	0.454
R_s	0.8Ω

where C_1, C_2, C_3, and C_4 are numerical constants, i, j, and k are integers ≥ 2, V_T is the threshold voltage (voltage below $V_{\rm peak}$ for which d^2I/dV^2 displays a local maximum), V_N is the voltage of the steepest part of the NDR region, and M is a multiplying factor. The parameters for the RTD model were calculated using the NonlinearFit function provided in Mathematica (the computer algebra system) to fit the RTD model to five data points (including $V_{\rm peak}$, $I_{\rm peak}$ and $I_{\rm valley}$, $V_{\rm valley}$) from the experimental RTD I–V characteristic. The parameters used are given in Table I.

The laser model is the one presented by Tsou *et al.* [19]. This model is a SPICE based equivalent circuit model of the optical and electrical properties of a single quantum well laser diode with a confinement heterostructure emitting at 980 nm. This model accurately represents the dynamical operating characteristics of the laser diode, however, only the dc characteristics are utilised here. The dc optical power versys current ($P_{\rm opt}$–I) characteristic of the laser diode model was made to fit the experimental $P_{\rm opt}$–I characteristic of the RTD-LD module laser diode by changing the value of a parameter RP, related to photon lifetime by $RP = \tau_p \bar{p}/q$ (where τ_p is a constant for converting photon population P to output power and q is the electronic charge) and by use of a scale factor (multiplication of the $P_{\rm opt}$–I characteristic by a constant—$C_{P_{\rm opt}}$). Series resistance of 0.8 Ω (extracted from the laser diode I–V characteristic) was also added to the model. Values are shown in Table II. The PSPICE netlist used for the simulation is given in appendix.

The RTD-LD module simulations without and with the inclusion of 15 Ω series resistance (15.8 Ω including the laser diode series resistance) are shown as dashed lines in Fig. 2 and and Figs. 5 and 6, respectively. The fits to the experimental data are generally close in both cases. Discrepancies do arise between $V_{\rm peak}$ and $V_{\rm valley}$ points in the simulation and experimental results for the zero external series resistance case that lead to differences in $V'_{\rm peak}$ and $V'_{\rm valley}$ values between model and experimental I–Vs with 15-Ω series resistance.

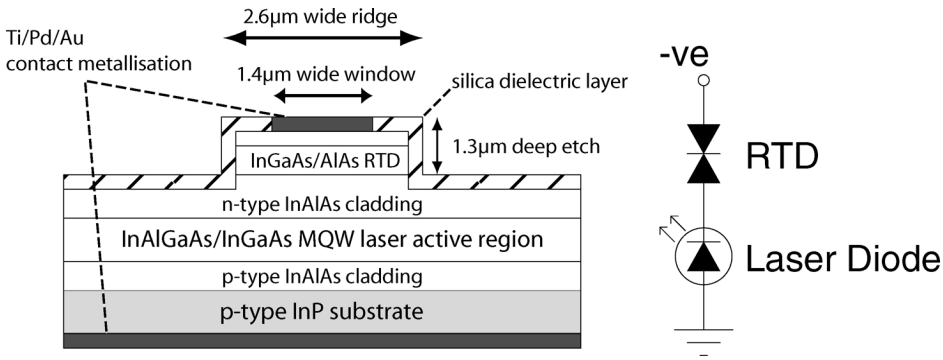

Fig. 7. Cross section (not to scale) of the layout of the ridge waveguide RTD Laser. Cavity length is 500 μm giving an RTD active area of 1300 μm^2. Alongside is a schematic circuit representation of the device.

III. Monolithically Integrated RTD-LD

A suitable epi-wafer for the device was grown by molecular beam epitaxy, and consisted of a resonant tunnelling diode grown above a multiple quantum well laser. The laser section was based on a design presented in [20] and consisted of six 6.7-nm-thick InGaAs quantum wells with 10-nm InGaAlAs barriers. The RTD consisted of a 5-nm InGaAs quantum well sandwiched by strained 2-nm AlAs barriers. The full epitaxial layer structure is given in Table III. Devices were fabricated based on the ridge waveguide laser design shown in Fig. 7. In order to control its active area, the RTD was situated in the waveguide ridge, between the laser section of the device and the n-type contact. The laser had a cavity length of 500 μm, and so with the 2.6-μm ridge width the RTD had an active area of 1300 μm^2. The laser active area was a minimum of 1300 μm^2, with the actual area dependent on the extent of current spreading beneath the ridge. RTDs usually operate with n-type material and therefore in this design it was necessary to use a p-type InP substrate.

At a temperature of 22 °C, the device gave laser emission only under pulsed current conditions (44-ns pulse length at 1-KHz rep rate) and with a threshold current of 306 mA and a central emission wavelength of 1540 nm. Given that this is a voltage controlled device with characteristics dependant on source resistance, a pulsed current source was not suitable to show the desired voltage controlled bistability exhibited by the RTD-LD module. In order to use the same CW voltage source used to characterise the RTD-LD module the integrated RTD-LD was cooled to allow CW laser operation.

The dc electrical and optical characteristics of the device are shown in Figs. 8 and 9. For epilayers up mounting of the RTD-LD, to obtain CW laser operation, it was necessary to operate the device at a temperature of 130 K. Optical simulations have shown that the high room temperature threshold current and necessarycooling for CW operation were at least due in part to optical losses in epilayer number 1 (Table III). We anticipate that with some improvement of the laser design and epilayer down mounting room temperature operation will be obtainable.

From Fig. 8, we can see that the device is electrically bistable and thereby optically bistable confirmed by Fig. 9. The width of the hysteresis loop is 1.3 V and so when dc biased to the middle of the loop a $> +0.65$ V pulse will switch the laser from *on* to *off* and a > -0.65 V pulse will switch the laser from *off* to *on*. The threshold current of the laser (77 mA) is represented by a dashed line in Fig. 8 and was taken from the optical power versus current curve in Fig. 10. The condition $I_{\rm peak} > I_{\rm th} > I_{\rm valley}$, is met in this case, leading to an extinction ratio of 15 dB in the laser output power between the *on* and *off* states when biased in the middle of the bistable region, so a +0.65 V pulse

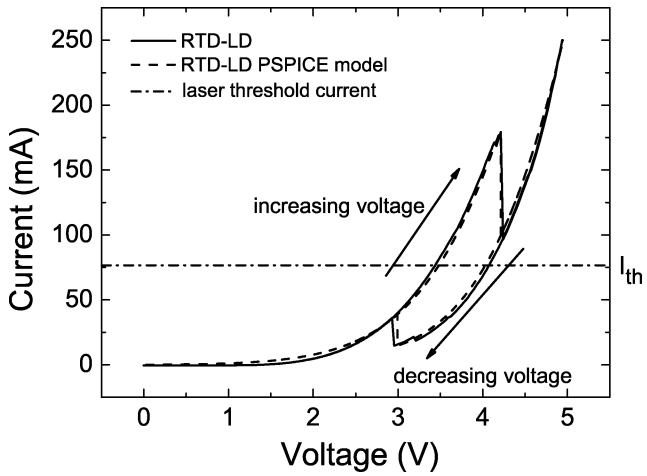

Fig. 8. Solid curves give the I–V characteristic for the RTD-LD at 130 K showing electrical bistability. The RTD peak and valley currents are 179 and 14.7 mA, respectively. The dashed horizontal line represents the threshold current of the laser. The SPICE model data is given by the dashed curves.

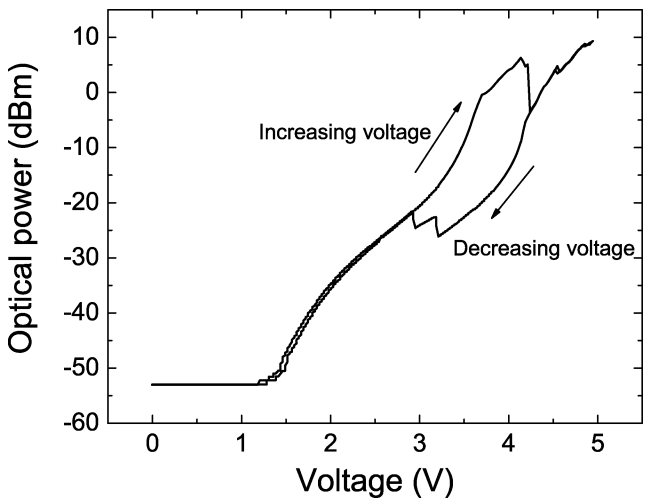

Fig. 9. $P_{\rm opt}$-V characteristic for the RTD-LD at 130 K showing optical bistability.

TABLE III
EPITAXIAL LAYER STRUCTURE OF THE MONOLITHICALLY INTEGRATED RTD-LD. QW: QUANTUM WELL; NID: NOT INTENTIONALLY DOPED

Layer number	Material	thickness (nm)	Doping (cm^{-3})	Details
Wafer	P-InP		$2*10^{18}$	
1	P-$In_{0.53}Ga_{0.47}As$	500	$5*10^{18}$	
2	P-$In_{0.52}Al_{0.48}As$	500	$5*10^{17}$	cladding
3	$In_{0.52}Al_{0.2}Ga_{0.27}As$	250	nid	core
4,6,8,10, 12,14	$In_{0.52}Al_{0.48}As$	6.7	nid	6 laser QWs
5,7,9,11, 13	$In_{0.52}Al_{0.2}Ga_{0.27}As$	9	nid	5 barriers
15	$In_{0.52}Al_{0.2}Ga_{0.27}As$	250	nid	core
16	N-$In_{0.52}Al_{0.48}As$	1000	$5*10^{17}$	cladding
17	N-$In_{0.53}Ga_{0.47}As$	100	$1*10^{18}$	
18	$In_{0.53}Ga_{0.47}As$	2	nid	spacer
19	AlAs	2.3	nid	barrier
20	$In_{0.53}Ga_{0.47}As$	5	nid	RTD QW
21	AlAs	2.3	nid	barrier
22	$In_{0.53}Ga_{0.47}As$	2	nid	spacer
23	N-$In_{0.53}Ga_{0.47}As$	100	$1*10^{18}$	
24	N-$In_{0.53}Ga_{0.47}As$	200	$5*10^{18}$	cap layer

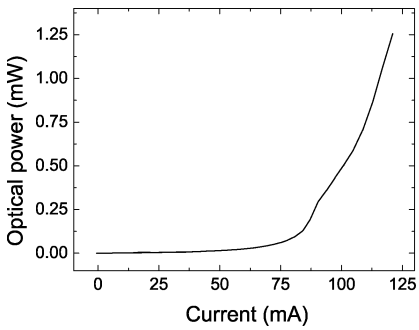

Fig. 10. $P_{\rm opt}$–I characteristic for the RTD-LD at 130 K. The laser threshold current is 77 mA.

can provide 15 dB of modulation. Furthermore with a bistable device non-return to zero modulation is more easily obtained.

Bistability in RTDs can arise for one of two reasons. The intrinsic bistability—where charge storage allows two different states of band bending for one applied bias—has been observed by Alves *et al.* [21] and explained theoretically in [22] and [23]. The extrinsic bistability is illustrated in the load line analysis of [10] and is caused by the presence of the laser diode and series resistance.

PSPICE was used to model the RTD-LD and determine if the observed bistability in Figs. 8 and 9 is explainable in terms of the extrinsic load line effect that produced the bistability observed in the RTD-LD module with series resistance. The electrical/optical HIC PSPICE model was simplified to take into account only the electrical RTD-LD behavior, and to this end, the laser diode model was replaced with the PSPICE diode model[2]

$$\begin{aligned} I_{\rm fwd} &= I_{\rm nrm} + I_{\rm rec}K_{gen} \\ I_{\rm nrm} &= I_{\rm s}(e^{v_d/N\cdot V_T} - 1) \\ I_{\rm rec} &= I_{\rm sr}(e^{v_d/N_r\cdot V_T} - 1). \end{aligned} \tag{2}$$

where $I_{\rm fwd}$ is the forward diode current,composed of both the normal current $I_{\rm nrm}$, and $I_{\rm rec}$, the recombination current. K_{gen} is the current generation factor. N, and N_r are the ideality factors, I_s and $I_{\rm sr}$ are the saturation currents and V_t is the thermal voltage. v_d is the diode voltage. Using a method presented in [24] whereby the gradient of an RTD I–V characteristic is measured at higher biases as it tends to the value $1/R_s$, the series resistance of the RTD-LD was found to be 1 Ω (at 130 K). This series resistance was added to the simulation.

[2]OrCAD PSPICE Reference Guide, 1999.

TABLE IV
DIODE MODEL PARAMETERS USED IN (2) FOR FITTING THE INTEGRATED RTD-LD PSPICE MODEL

Diode model parameter	Value
I_s	$1.25*10^{-32}A$
N	4.64
I_{sr}	$2.15*10^{-4}A$
N_r	41.79
V_T	11.2mV

TABLE V
RTD MODEL PARAMETERS USED IN (1) FOR FITTING THE INTEGRATED RTD-LD PSPICE MODEL

RTD model Parameter	Value
i	3
j	5
k	4.5
C1	$3.54*10^{-4}$
C2	100
C3	$1.02*10^{-3}$
C4	$-1.00*10^{-3}$
V_T	0V
V_N	0.93V
Scale	256

The diode model parameters were adjusted along with those of the RTD model using trial and error along with the NonlinearFit function provided in Mathematica to give the best possible fit to the experimental RTD-LD I–V characteristic. Fig. 8 shows the actual RTD-LD I–V characteristic overlaid with the simulation results obtained using the diode and RTD parameters given in Tables IV and V. The simulation results are consistent with the load line effect being the cause of the bistability in the RTD-LD.

The diode parameters used in Table IV to achieve the fit are notably different to those found for typical diodes. Though it is not unusual to see a wide range of saturation currents depending on device size etc, the values of ideality factor (5 and 42) fall well without the typical range (normally 1–2 [25]). These parameters give the diode model a "high" (20 Ω) differential resistance at lower biases (0 to around 5 V) and "low" (1 Ω as the I–V tends to $1/R_S$) resistance at higher biases and hence in series with the RTD I–V gives a wide hysteresis loop while presenting a low measured series resistance. Another factor contributing to the hysteresis loop width is the large value of RTD peak current which in combination with the series resistance, increases the value of $V_{\rm peak}$ [26].

To explain the origin of the non-linear loadline behavior we undertook an investigation of the contacts; a particular aim was to understand and reduce the width of the hysteresis curve. The bottom, P-type contact of Ti–Pd–Au was changed to Zn–Au, with the aim of producing a more ohmic contact [27], however the device still exhibited a wide hysteresis loop and so this aspect of the device requires further investigation.

```
Netlist for DC RTD-LD PSPICE simulation

*RTD  equation
G_ABM2I1          N00504 N22643 VALUE
+  Scale*C1*(V(N00504) - V(N22643))**i*
+ ATAN(C2*(V(N00504) - V(N22643))-VTh)-
+ ATAN(C2*(V(N00504) - V(N22643))-VN)+
+ C3*(V(N00504) - V(N22643))**j+C4*
+ (V(N00504) - V(N22643))**k


*RTD parallel capacitance
C_C1          N22643 N00504  60f


*Laser diode model
X_U1          N22643 LD model


*Voltage source- DC
V_V1          N56355 0 0Vdc


*Series resistance
R_R1          N00504 N56355  RES


*Various parameters for RTD model equation
*and series resistance value
.PARAM C1=0.075 C2=3.215 C3=0.023
+ C4=-0.051 i=1 j=2 k=1 VN=1.01 VTh=0
+ Scale=1 RES=15

.SUBCKT LD model 31
*EQUIVALENT CIRCUIT FOR A QUANTUM-WELL
*LASER
*SCH=300NM

*DEFINE A FUNCTION LIMITING OUTPUT
*POWER TO POSITIVE VALUE ONLY
.FUNC LIM(X)  LIMIT(X,0,50E-3)

*MATERIAL GAIN FOR QW
.PARAM A0=-771899.99, A1=34220.10,
+ A2=-376.83
.FUNC G(X) A0+(A1*LOG(X))+
+ (A2*LOG(X)*LOG(X))
```

Fig. 11. PSPICE netlist for RTD-LD module simulation—Part 1.

The optical spectra for the device at 130 K has a central peak at a wavelength of 1476 nm. The 130-K operating temperature shifted the emission peak to a shorter wavelength than the room temperature wavelength of 1540 nm.

The device can be improved by refinement of the laser section design in combination with epilayer down mounting to enable room temperature operation and a lower threshold current. In addition, with an improved RTD design, I_{peak} and I_{valley} will be decreased in line with I_{th} in order to maintain the condition $I_{\text{peak}} > I_{\text{th}} > I_{\text{valley}}$.

```
*PARAMETERS FOR THE CIRCUIT MODEL
.PARAM R_PH=0.362, C_PH=5.2827E-12,
+ EV=2.0882,
+ BEFF=1E-4
.PARAM TESC=200E-12, TD=48.263E-12,
+ TC=0.18E-12, TG=1E-12
.PARAM TNS=1E-9, TNQ=0.35E-9, TNG=1E-9
.PARAM RATIO1=TNS/TD, RATIO2=TNG/TG,
+ RATIO3=TNG/TC, RATIO4=TNQ/TESC
.PARAM ISS=6.66E-15, ISG=4.57E-16,
+ ISQ=1.208E-13

*DEFINE SOME COEFFICIENTS USED IN THE
*CIRCUIT
.PARAM COEFF1=TNQ*1.040249E30;(TNQ/(Q*VQ))
.PARAM COEFF2=7.5450E-4;(Q*GAMMA*VG/PBAR)

***** BEGIN CIRCUIT *****

*SCH SECTION
VIS 3 4 DC 0
.MODEL DSCH D (IS=ISS N=2 RS=0.45)
DS 4 0 DSCH
G1 3 0 VALUE=I(VI1)

*DERIVATIVE CIRCUIT FOR SCH
E1 21 0 VALUE=I(VIS)
VI1 21 22 DC 0
C1 22 0 TNS

*SCH ---> GATE
G2 3 5 VALUE=RATIO1*I(VIS)
G3 5 3 VALUE=RATIO2*I(VIG)

*GATEWAY SECTION
VIG 5 6 DC 0
.MODEL DGATE D (IS=ISG N=2 RS=15)
DG 6 0 DGATE
G4 5 0 VALUE=I(VI2)

*DERIVATIVE CIRCUIT FOR GATE
E2 23 0 VALUE=I(VIG)
VI2 23 24 DC 0
C2 24 0 TNG

*GATE ---> QW
G5 5 7 VALUE=RATIO3*I(VIG)
G6 7 5 VALUE=RATIO4*I(VIQ)

*QW SECTION
VIQ 7 8 DC 0
.MODEL DQW D (IS=ISQ N=2 RS=10)
DQ 8 0 DQW
G7 7 0 VALUE=I(VI3)

*DERIVATIVE CIRCUIT FOR QW
E3 25 0 VALUE=I(VIQ)
```

Fig. 12. PSPICE netlist for RTD-LD module simulation—Part 2.

IV. Conclusion

We have demonstrated the operation of a bistable monolithically integrated RTD-LD and have modelled its operation using

```
VI3 25 26 DC 0
C3 26 0 TNQ

*STIMULATED EMISSION SECTION
GSTIM 7 9 VALUE=(COEFF2*G(COEFF1*I(VIQ))*
+ LIM(V(9,0)))/(SQRT(1+EV*LIM(V(9,0))))
GSPON 0 9 VALUE=BEFF*I(VIQ)
RP 9 0 R_PH
CP 9 0 C_PH

*SOURCE, PACKAGE, AND INTERNAL PARASITICS
CJ 3 0 0.1405PF
CB 31 0 0.1P
LB 31 33 0.002N

CS 33 34 1.6P
RSUB 34 0 1.5
RS 33 3 0.8
.ENDS

*Simulation commands
.DC LIN V_V1 0 4 0.005
.OPTIONS STEPGMIN
.PROBE V(*) I(*) W(*) D(*) NOISE(*)

.END
```

Fig. 13. PSPICE netlist for RTD-LD module simulation—Part 3.

a PSPICE simulation validated from measurements taken on an HIC. The PSPICE model was modified to take into account only the electrical RTD-LD behavior, and using suitable fitting parameters, was a close fit to the electrical RTD-LD behavior.

Because it makes use of the vertical stacking arrangement of the layers that make up an optical communications laser the integration of a RTD is a relative simple addition to the laser.

Furthermore, from work presented elsewhere [28], we know that a top end estimate for a RTD-LD operating in the high optical power state the RTD presents a thermal load on the laser resulting in a 17 °C increase in laser active region temperature and a factor of 1.2 increase in laser threshold current. Providing that the change in threshold current does not cause the condition $I_{\mathrm{peak}} > I_{\mathrm{th}} > I_{\mathrm{valley}}$ to be violated the device performance should not be significantly affected by the additional thermal load.

In more general terms, we have outlined a methodology for developing OEICs. First a HIC is constructed from components similar to the components in the target integrated device; with the HIC each component can be separately characterised and the results fed into a PSPICE model of the HIC which is adjusted to fit the measurements of the key parameters describing operation of the HIC. This model can then be applied to the integrated device.

We believe that this integrated RTD-LD can find application in digital optical communication systems because inherently it suitable for digital switching. However, to achieve this aim more work is required on several aspects of the device. These include high frequency operation and characterisation, reduction of hysteresis width in order to decrease the required drive voltage, and implementation of a circuit to combine RTD dc bias voltage and drive signal.

APPENDIX
PSPICE NETLIST FOR RTD-LD MODULE SIMULATION

See Figs. 11–13. Parts of the netlist pertaining to the laser diode model are reproduced from [19].

ACKNOWLEDGMENT

The authors would like to thank C. Farmer for help with the RTD-LD characterization and in addition M. Hopkinson and C. Stanley for MBE material growth. They also thank Intense, Ltd., U.K., for the donation of a suitable semiconductor laser.

REFERENCES

[1] L. L. Chang, L. Esaki, and R. Tsu, "Resonant tunneling in semiconductor double barriers," *Appl. Phys. Lett.*, vol. 24, no. 12, pp. 593–595, 1974.

[2] P. R. Berger, N. K. Dutta, D. L. Sivco, and A. Y. Cho, "GaAs quantum-well laser and heterojunction bipolar-transistor integration using molecular-beam epitaxial regrowth," *Appl. Phys. Lett.*, vol. 59, no. 22, pp. 2826–2828, 1991.

[3] T. R. Chen, K. Utaka, Y. Zhuang, Y. Y. Liu, and A. Yariv, "A vertical monolithic combination of an InGaAsP–InP laser and a heterojunction bipolar-transistor," *IEEE J. Quantum Electron.*, vol. 23, no. 6, pp. 919–924, Jun. 1987.

[4] S. Y. Chung, S. Y. Park, J. W. Daulton, R. H. Yu, P. R. Berger, and P. E. Thompson, "Integration of Si SiGe HBT and Si-based RITD demonstrating controllable negative differential resistance for wireless applications," *Solid-State Electron.*, vol. 50, no. 6, pp. 973–978, 2006.

[5] A. R. Bonnefoi, T. C. McGill, and R. D. Burnham, "Resonant tunneling transistors with controllable negative differential resistances," *IEEE Electron Device Lett.*, vol. EDL-6, no. 12, pp. 636–638, Dec. 1985.

[6] C. Vanhoof, J. Genoe, R. Mertens, G. Borghs, and E. Goovaerts, "Electroluminescence from bipolar resonant tunneling diodes," *Appl. Phys. Lett.*, vol. 60, no. 1, pp. 77–79, 1992.

[7] J. M. L. Figueiredo, C. N. Ironside, and C. R. Stanley, "Electric field switching in a resonant tunneling diode electroabsorption modulator," *IEEE J. Quantum Electron.*, vol. 37, no. 12, pp. 1547–1552, Dec. 2001.

[8] Y. Kawamura, H. Asai, and H. Iwamura, "Fabrication of resonant-tunneling optical bistable laser-diodes," *Electron. Lett.*, vol. 30, no. 3, pp. 225–227, 1994.

[9] C. R. Lutz, F. Agahi, and K. M. Lau, "Resonant-tunneling injection quantum-well lasers," *IEEE Photon. Technol. Lett.*, vol. 7, no. 6, pp. 596–598, Jun. 1995.

[10] I. Grave, S. Kan, G. Griffel, S. Wu, A. Saar, and A. Yariv, "Monolithic integration of a resonant tunneling diode and a quantum-well semiconductor-laser," *Appl. Phys. Lett.*, vol. 58, no. 2, pp. 110–112, 1991.

[11] G. W. Roberts and A. S. Sedra, *SPICE*, 2nd ed. Oxford, U.K.: Oxford Univ. Press, 1997.

[12] T. J. Slight, C. N. Ironside, C. R. Stanley, M. Hopkinson, and C. D. Farmer, "Integration of a resonant tunneling diode and an optical communications laser," *IEEE Photon. Technol. Lett.*, vol. 18, no. 14, pp. 1518–1520, Jul. 2006.

[13] Y. Takahashi, T. Kato, and D. H. Hartman, "A subminiaturized LD transmitter module for 2.4 Gb/s transmission," *IEEE Photon. Technol. Lett.*, vol. 3, no. 5, pp. 471–472, May 1991.

[14] T. Suzaki, Y. Suzuki, H. Yamada, S. Fujita, H. Hida, M. Kitamura, and M. Shikada, "10 Gbit/s optical transmitter module with MQW DFB-LD and DTM driver IC," *Electron. Lett.*, vol. 26, no. 2, pp. 151–152, 1990.

[15] M. Menouni, E. Wawrzynkowski, S. Vuye, P. Desrousseaux, P. Launay, and J. Dangla, "14 Gbit/s digital optical transmitter module using GaAs HBTs and DFB laser," *Electron. Lett.*, vol. 32, no. 3, pp. 231–233, 1996.

[16] C. Y. Belhadj, K. P. Martin, S. Benamor, J. J. L. Rascol, R. J. Higgins, R. C. Potter, H. Hier, and E. Hempfling, "Bias circuit effects on the current-voltage characteristic of double-barrier tunneling structures – Experimental and theoretical results," *Appl. Phys. Lett.*, vol. 57, no. 1, pp. 58–60, 1990.

[17] M. Q. Bao and K. L. Wang, "Accurately measuring current-voltage characteristics of tunnel diodes," *IEEE Trans. Electron Devices*, vol. 53, no. 10, pp. 2564–2568, Oct. 2006.

[18] E. R. Brown, O. B. McMahon, L. J. Mahoney, and K. M. Molvar, "Spice model of the resonant-tunnelling diode," *Electron. Lett.*, vol. 32, no. 10, pp. 938–940, 1996.
[19] B. P. C. Tsou and D. L. Pulfrey, "A versatile Spice model for quantum-well lasers," *IEEE J. Quantum Electron.*, vol. 33, no. 2, pp. 246–254, Feb. 1997.
[20] M. Jain, "An investigation of broad gain spectrum InGaAs/InAlGaAs quantum well lasers latticed matched to InP," Ph.D. dissertation, Dept. Electron. Elect. Eng., Univ. Glasgow, Glasgow, U.K., 2002.
[21] E. S. Alves, L. Eaves, M. Henini, O. H. Hughes, M. L. Leadbeater, F. W. Sheard, G. A. Toombs, G. Hill, and M. A. Pate, "Observation of intrinsic bistability in resonant tunnelling devices," *Electron. Lett.*, vol. 24, no. 18, pp. 1190–1191, 1988.
[22] F. W. Sheard and G. A. Toombs, "Space-charge buildup and bistability in resonant-tunneling double-barrier structures," *Appl. Phys. Lett.*, vol. 52, no. 15, pp. 1228–1230, 1988.
[23] M. Rahman and J. H. Davies, "Theory of intrinsic bistabillity in a resonant tunneling diode," *Semicond. Sci. Technol.*, vol. 5, no. 2, pp. 168–176, 1990.
[24] M. J. Deen, "Simple method to determine series resistance and its temperature-dependence in AlAs/GaAs/AlAs double barrier resonant tunneling diodes," *Electron. Lett.*, vol. 28, no. 13, pp. 1195–1197, 1992.
[25] S. Sze, *Semiconductor Devices—Physics and Technology*. New York: Wiley, 2002, p. 112.
[26] N. Jin, S. Y. Chung, A. T. Rice, P. R. Berger, R. H. Yu, P. E. Thompson, and R. Lake, "151 kA/cm^2 peak current densities in Si SiGe resonant interband tunneling diodes for high-power mixed-signal applications," *Appl. Phys. Lett.*, vol. 83, no. 16, pp. 3308–3310, 2003.
[27] V. Malina, U. Schade, and K. Vogel, "Technological aspects of the preparation of Au–Zn ohmic contacts to P-Type InP," *Semicond. Sci. Technol.*, vol. 9, no. 1, pp. 49–53, 1994.
[28] T. J. Slight, "Integration of a resonant tunnelling diode and an optical communications laser," Ph.D. dissertation, Dept. Electr. Elect. Eng., Univ. Glasgow, Glasgow, U.K., 2006.

Thomas J. Slight received the B.Eng. degree in physics and electronic engineering and the Ph.D. degree in electronic engineering from the University of Glasgow, Glasgow, U.K., in 2002 and 2006, respectively.

He is currently with the Department of Electronics and Electrical Engineering, University of Glasgow, where his research interests include optoelectronic integrated circuits utilizing resonant tunnelling diodes.

Charles N. Ironside has worked in the Department of Electronics and Electrical Engineering, University of Glasgow, Glasgow, U.K., since 1984, on a variety of optoelectronic projects that include: ultrafast all-optical switching in semiconductor waveguides; monolithic mode-locked semiconductor lasers; broad-band semiconductor lasers; quantum-cascade lasers; and optoelectronic integrated chip (OEIC) devices. His OEIC work has concentrated on the integration of resonant tunnelling diodes with electroabsorption modulators and semiconductor lasers.